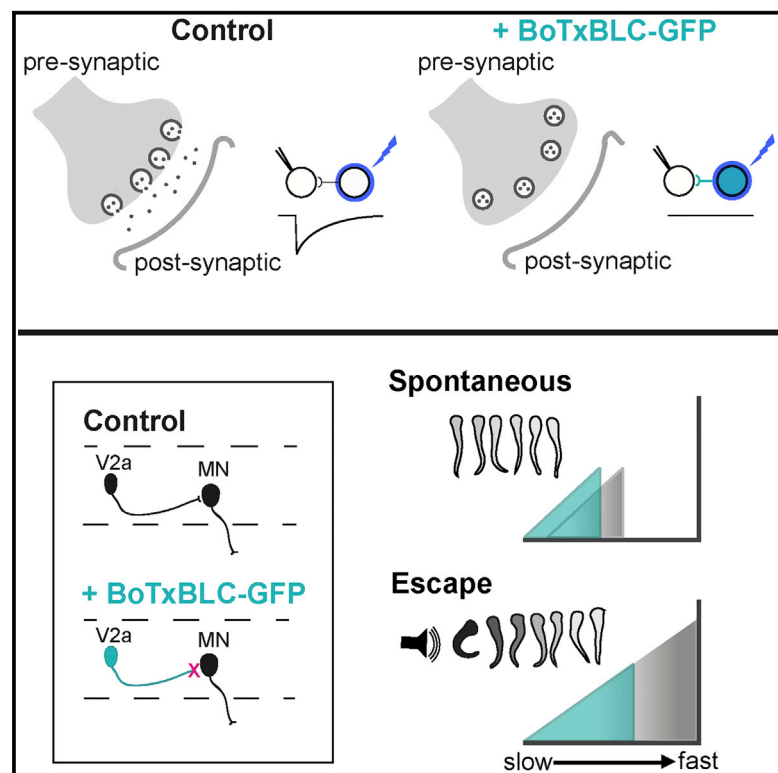


Current Biology

Optimization of a Neurotoxin to Investigate the Contribution of Excitatory Interneurons to Speed Modulation In Vivo

Graphical Abstract



Authors

Jenna R. Sternberg, Kristen E. Severi, Kevin Fidelin, ..., Koichi Kawakami, Maximiliano Suster, Claire Wyart

Correspondence

kokawaka@nig.ac.jp (K.K.),
claire.wyart@icm-institute.org (C.W.)

In Brief

Silencing of neuronal populations in moving animals remains a challenge to investigating neural control of behavior. By developing an optimized botulinum toxin to block synaptic release in vivo, Sternberg, Severi et al. show that excitatory V2a interneurons contribute to locomotor frequency in distinct ways during slow or fast locomotion.

Highlights

- Optimized, genetically encoded botulinum neurotoxin silences synaptic output in vivo
- Excitatory V2a interneurons drive high-frequency components of fast locomotion
- Silencing of V2as shifts locomotor frequency downward during the slow regime



Optimization of a Neurotoxin to Investigate the Contribution of Excitatory Interneurons to Speed Modulation In Vivo

Jenna R. Sternberg,^{1,2,3,4,8} Kristen E. Severi,^{1,2,3,4,8} Kevin Fidelin,^{1,2,3,4} Johanna Gomez,^{1,2,3,4} Hideshi Ihara,⁵ Yara Alcheikh,^{1,2,3,4} Jeffrey M. Hubbard,^{1,2,3,4} Koichi Kawakami,^{6,*} Maximiliano Suster,^{6,7} and Claire Wyart^{1,2,3,4,*}

¹Institut du Cerveau et de la Moelle Épineuse (ICM), 47 Boulevard de l'Hôpital, 75013 Paris, France

²INSERM UMRS 1127, 75013 Paris, France

³CNRS UMR 7225, 75013 Paris, France

⁴UPMC Université Paris 06, 75005 Paris, France

⁵Department of Biological Science, Graduate School of Science, Osaka Prefecture University, Sakai, Osaka 599-8531, Japan

⁶Division of Molecular and Developmental Biology, National Institute of Genetics, and Department of Genetics, SOKENDAI (The Graduate University for Advanced Studies), Mishima, Shizuoka 411-8540, Japan

⁷Neural Circuits and Behaviour Group, Uni Research AS, Thormøhlensgate 55, Bergen 5008, Norway

⁸Co-first author

*Correspondence: kokawaka@nig.ac.jp (K.K.), claire.wyart@icm-institute.org (C.W.)

<http://dx.doi.org/10.1016/j.cub.2016.06.037>

SUMMARY

Precise control of speed during locomotion is essential for adaptation of behavior in different environmental contexts [1–4]. A central question in locomotion lies in understanding which neural populations set locomotor frequency during slow and fast regimes. Tackling this question in vivo requires additional non-invasive tools to silence large populations of neurons during active locomotion. Here we generated a stable transgenic line encoding a zebrafish-optimized botulinum neurotoxin light chain fused to GFP (BoTxBLC-GFP) to silence synaptic output over large populations of motor neurons or interneurons while monitoring active locomotion. By combining calcium imaging, electrophysiology, optogenetics, and behavior, we show that expression of BoTxBLC-GFP abolished synaptic release while maintaining characterized activity patterns and without triggering off-target effects. As *chx10*⁺ V2a interneurons (V2as) are well characterized as the main population driving the frequency-dependent recruitment of motor neurons during fictive locomotion [5–14], we validated our silencing method by testing the effect of silencing *chx10*⁺ V2as during active and fictive locomotion. Silencing of V2as selectively abolished fast locomotor frequencies during escape responses. In addition, spontaneous slow locomotion occurred less often and at frequencies lower than in controls. Overall, this silencing approach confirms that V2a excitation is critical for the production of fast stimulus-evoked swimming and also reveals a role for V2a excitation in the production of slower spontaneous locomotor behavior. Altogether, these results establish BoTxBLC-GFP

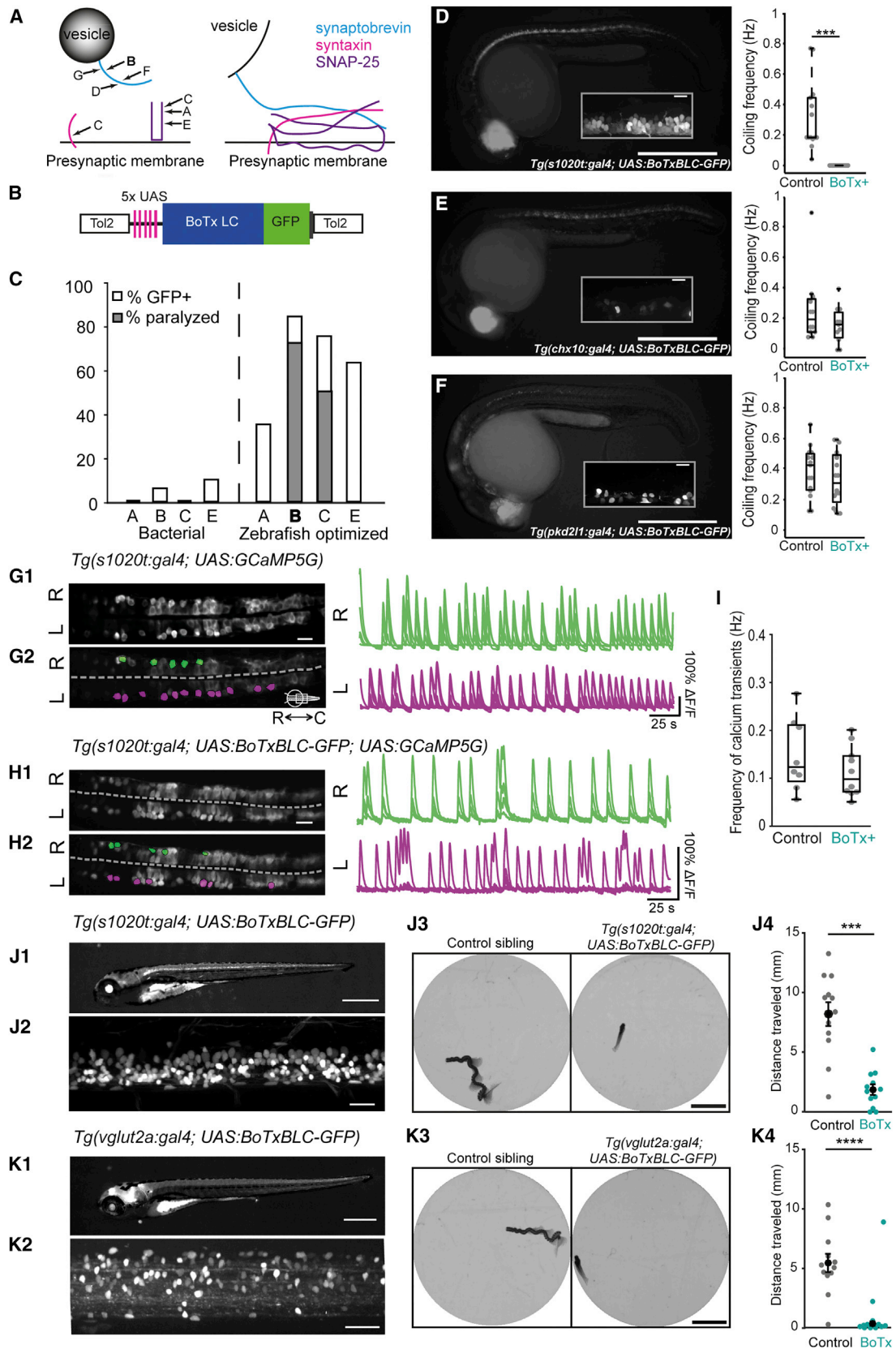
as an ideal tool for in vivo silencing for probing the development and function of neural circuits from the synaptic to the behavioral level.

RESULTS

Generation of a Zebrafish-Optimized Transgenic Line for Botulinum Neurotoxin Light Chain

In order to understand the neural circuits underlying behavior, efficient tools to silence distinct classes of neurons in behaving animals are necessary. Botulinum toxins are potent poisons that block vesicular release at the synaptic cleft by cleaving SNARE (soluble NSF attachment protein [SNAP] receptor) proteins and thus eliminate synaptic transmission [15–18]. The efficacy and specificity of action of botulinum toxin light chains (BoTxLCs) make them ideal tools for silencing neurons. However, stable transgenic lines optimized for expression have not yet been generated and characterized in zebrafish.

We utilized the two-part Gal4/UAS combinatorial gene expression system [19, 20] to generate a stable and efficient zebrafish-optimized transgenic line encoding BoTxLC fused to GFP to abolish synaptic release in vivo. To test the efficiency of neuronal silencing of different botulinum neurotoxin serotypes (Figure 1A), we expressed distinct serotypes fused to GFP under the control of a 5× repeat of UAS (Figure 1B). We quantified the touch escape response of embryos transiently expressing either the bacterial or zebrafish codon-optimized variants of each serotype under a ubiquitous driver (Figure 1C) [19]. The bacterial forms were unable to induce paralysis, whereas the zebrafish codon-optimized form of the B serotype paralyzed 72% of embryos (Figure 1C). We established a stable transgenic line for the B serotype, *Tg(UAS:BoTxBLC-GFP)*. Offspring of *Tg(UAS:BoTxBLC-GFP)* fish mated to *Tg(SAGFF73A:gal4)* fish [19] (Table S1), which expresses ubiquitously, were unable to generate spontaneous and touch-evoked movement (>99%; data not shown). *Tg(UAS:BoTxBLC-GFP)* fish of at least the tenth generation were used for the remainder of this article.



(legend on next page)

Expression of BoTxBLC-GFP in Spinal Motor Neurons Selectively Abolishes Coiling at the Embryonic Stage

To test the efficiency and evaluate off-target effects of BoTxBLC-GFP, we performed a behavioral assay using Gal4 lines driving expression in either motor neurons or spinal interneurons [5, 20, 21]. Embryos 17–25 hr post-fertilization (hpf) perform a gap junction driven stereotyped coiling behavior [22, 23]. To determine whether BoTxBLC-GFP expressed in motor neurons could block muscle contraction, we used *Tg(s1020t:gal4)*, which drives expression in a large subset of motor neurons [24, 25] (Figure S1). Embryos lost the ability to coil when BoTxBLC-GFP was expressed in this line (Figure 1D; Movie S1). We then went on to test Gal4 lines expressing in interneurons that do not drive embryonic coiling [23]. Coiling persisted when embryos expressed BoTxBLC-GFP in *chx10*⁺ interneurons (*V2as*) or in GABAergic *pkd2l1*⁺ cerebrospinal-fluid-contacting neurons (CSF-cNs) (Figures 1E and 1F) [14, 26]. Together, these results indicate that BoTxBLC-GFP efficiently blocks synaptic output without off-target effects in zebrafish embryos.

BoTxBLC-GFP-Expressing Motor Neurons Maintain Their Characteristic Activity

To test whether the loss of coiling in *Tg(s1020t:gal4; UAS:BoTxBLC-GFP)* embryos (Figure 1D) was due to off-target effects of BoTxBLC-GFP expression, we performed calcium imaging in motor neurons expressing both BoTxBLC-GFP and GCaMP5G [21, 27, 28] (Figures 1G and 1H). Motor neurons in *Tg(s1020t:gal4; UAS:BoTxBLC-GFP; UAS:GCaMP5G)* embryos showed calcium transients occurring at comparable frequencies to non-BoTxBLC-GFP-expressing *Tg(s1020t:gal4; UAS:GCaMP5G)* embryos at 24 hpf (Figures 1G–1I; Movie S2).

This result indicates that expression of BoTxBLC-GFP silenced motor output without noticeably affecting motor neuron properties, suggesting that paralysis resulted from a loss of presynaptic release rather than cell death.

BoTxBLC-GFP Expression in Essential Neuronal Populations Effectively Disrupts the Escape Response in Freely Swimming Larvae

To test the utility of BoTxBLC-GFP in an active behavioral assay, we measured the escape response to an acoustic stimulus, which at 5 days post-fertilization (dpf) consists of a high amplitude turn followed by fast swimming [29, 30]. The expression of BoTxBLC-GFP in *Tg(s1020t:gal4)* (Figures 1J and S1), targeting a large subset of motor neurons, or in *Tg(vglut2a:gal4)*, targeting glutamatergic neurons (Figure 1K) [31], severely disrupted the escape response (Movie S3). When the larva responded, the distance traveled was significantly reduced (Figures 1J4 and 1K4), confirming that expression of BoTxBLC-GFP in essential motor circuit populations leads to a predictable massive deficit in locomotion at larval stages.

BoTxBLC-GFP Completely Blocks Synaptic Release In Vivo

To directly test the capacity of BoTxBLC-GFP to abolish vesicular release, we took advantage of a reliable monosynaptic connection between GABAergic CSF-cNs and caudal primary motor neurons (CaPs) (J.M.H., unpublished data). Using transgenic *Tg(pkd2l1:gal4; UAS:ChR2-mCherry)* larvae, we elicited single spikes with a 5 ms light pulse in CSF-cNs while performing whole-cell recordings in CaPs [21, 26] (Figures 2A and 2B). Light-mediated spiking of CSF-cNs induced large short-latency inhibitory postsynaptic currents (IPSCs) in CaPs (J.M.H., unpublished

Figure 1. Generation and Validation of the Transgenic Line *Tg(UAS:BoTxBLC-GFP)*

(A) Botulinum serotype B targets synaptobrevin, a SNARE complex protein essential for neurotransmitter release (after [17, 18]; A–G denote cleavage sites of distinct Botulinum serotypes).

(B) Design of the zebrafish codon-optimized *UAS:BoTxLC-GFP* constructs for the A, B, C, and E serotypes tested in transient.

(C) Percentage of *Tg(SAGFF73:gal4)* embryos paralyzed upon transient expression of BoTx serotypes, with and without codon optimization for zebrafish (embryos tested, from left to right: n = 11, 16, 18, 20, 20, 25, 16, and 30).

(D) Expression pattern of *Tg(s1020t:gal4; UAS:BoTxBLC-GFP)* double transgenic embryos (left) and reduction in coiling frequency (right). n = 14 BoTxBLC-GFP⁺ embryos and n = 14 control siblings.

(E) Same as (D) but for *Tg(chx10:gal4; UAS:BoTxBLC-GFP)*. n = 11 BoTxBLC-GFP⁺ embryos and n = 12 control siblings.

(F) Same as (D) but for *Tg(pkd2l1:gal4; UAS:BoTxBLC-GFP)*. n = 16 BoTxBLC-GFP⁺ embryos and n = 15 control siblings.

(G and H) Representative examples of calcium imaging in *Tg(s1020t:gal4; UAS:GCaMP5G)* control (G) and *Tg(s1020t:gal4; UAS:GCaMP5G; UAS:BoTxBLC-GFP)*

(H) embryos. Imaging plane (G1 and H1) and selected regions of interest (ROIs) (G2 and H2) (left and right hemispheres are indicated in magenta and green, respectively) are shown, with the corresponding $\Delta F/F$ traces on the right. Differences in $\Delta F/F$ amplitude result from higher levels of baseline GFP expression in BoTxBLC-GFP⁺ embryos.

(I) Frequency of calcium transients in control and BoTxBLC-GFP⁺ embryos. Each point represents the average frequency of all ROIs within an embryo (n = 8 BoTxBLC-GFP⁺ and n = 8 non-sibling control embryos).

(J) Comparison of control siblings and *Tg(s1020t:gal4; UAS:BoTxBLC-GFP)* 5 dpf larvae in a freely swimming acoustic escape assay. Whole-larva lateral view (J1), lateral view of the spinal cord (J2), and trajectories of swimming larvae in the assay (J3) are shown. Control siblings are *Tg(UAS:BoTxBLC-GFP)* only. (J4) shows the average distance traveled during a responsive trial (in millimeters) (n = 12 control larvae, 109 responses out of 118 trials; n = 11 BoTxBLC-GFP⁺ larvae, 72 responses out of 118 trials).

(K) Same as (J) but for *Tg(vglut2a:gal4; UAS:BoTxBLC-GFP)*. n = 12 control larvae, 98 responses out of 128 trials; n = 10 BoTxBLC-GFP⁺ larvae, 67 responses out of 128 trials.

Control sibling embryos for (D)–(F) had the Gal4, the UAS, or neither transgene. Insets for (D)–(F) are z projection stacks of a few optical sections imaged on the lateral side between segments 7 and 10. Scale bars represent 500 μ m in (D)–(F), 20 μ m for the insets in (D)–(F), 20 μ m in (G) and (H), 100 μ m in (J1) and (K1), 25 μ m in (J2) and (K2), and 5 mm in (J3) and (K3). (D)–(F), (J1), (J2), (K1), and (K2) are lateral views with dorsal up. (G) and (H) are dorsal views. Rostral is to the left in all panels. In (D)–(F), individual points correspond to coiling frequency for one embryo. For (J4) and (K4), the average responses of each larva are represented by a single gray point for control or teal point for BoTxBLC-GFP⁺ larvae, respectively. Means are shown \pm SEM in black. The central line on each boxplot is the median value, and the box limits are the 25th and 75th percentiles. The whiskers include all data points not considered outliers. ***p < 0.001, ****p < 0.0001, Student's t test (D–F and I). L, left; R, right. See also Figure S1, Table S1, and Movies S1, S2, and S3.

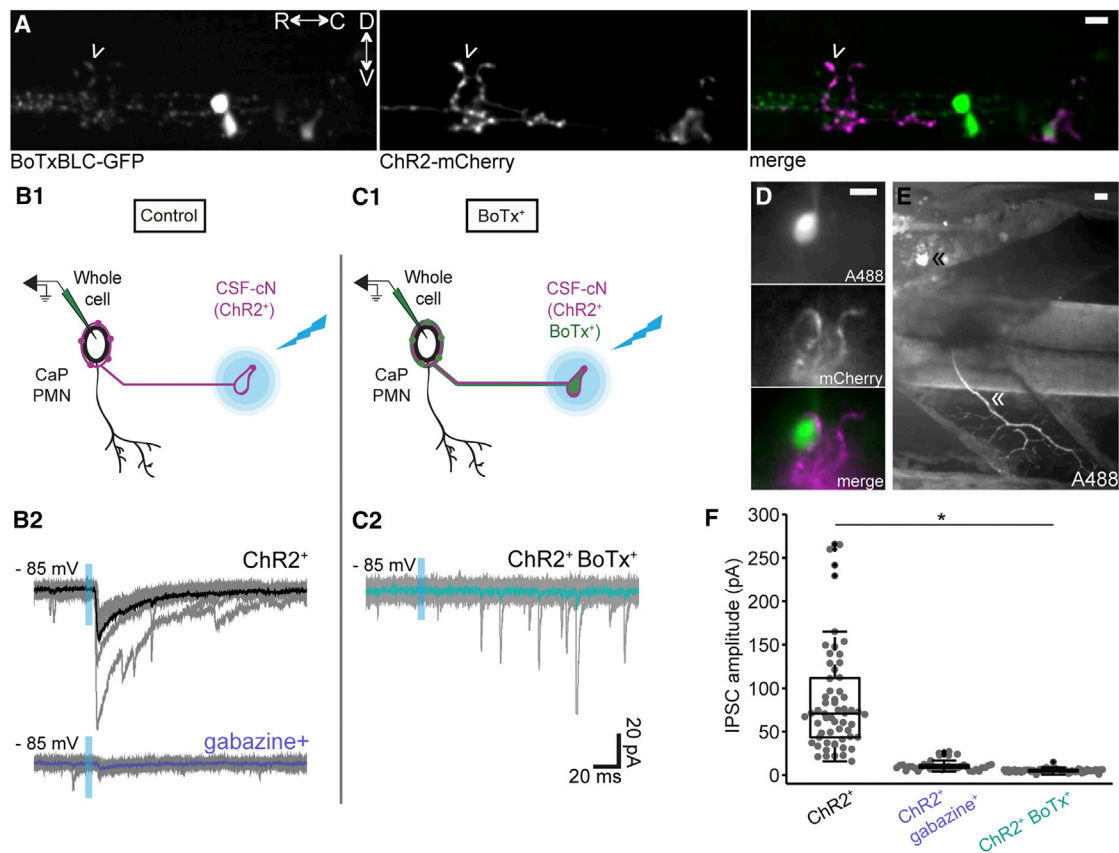


Figure 2. ChR2-Mediated Activation of Presynaptic Neurons Expressing BoTxBLC-GFP Demonstrates a Complete Block of Synaptic Release In Vivo

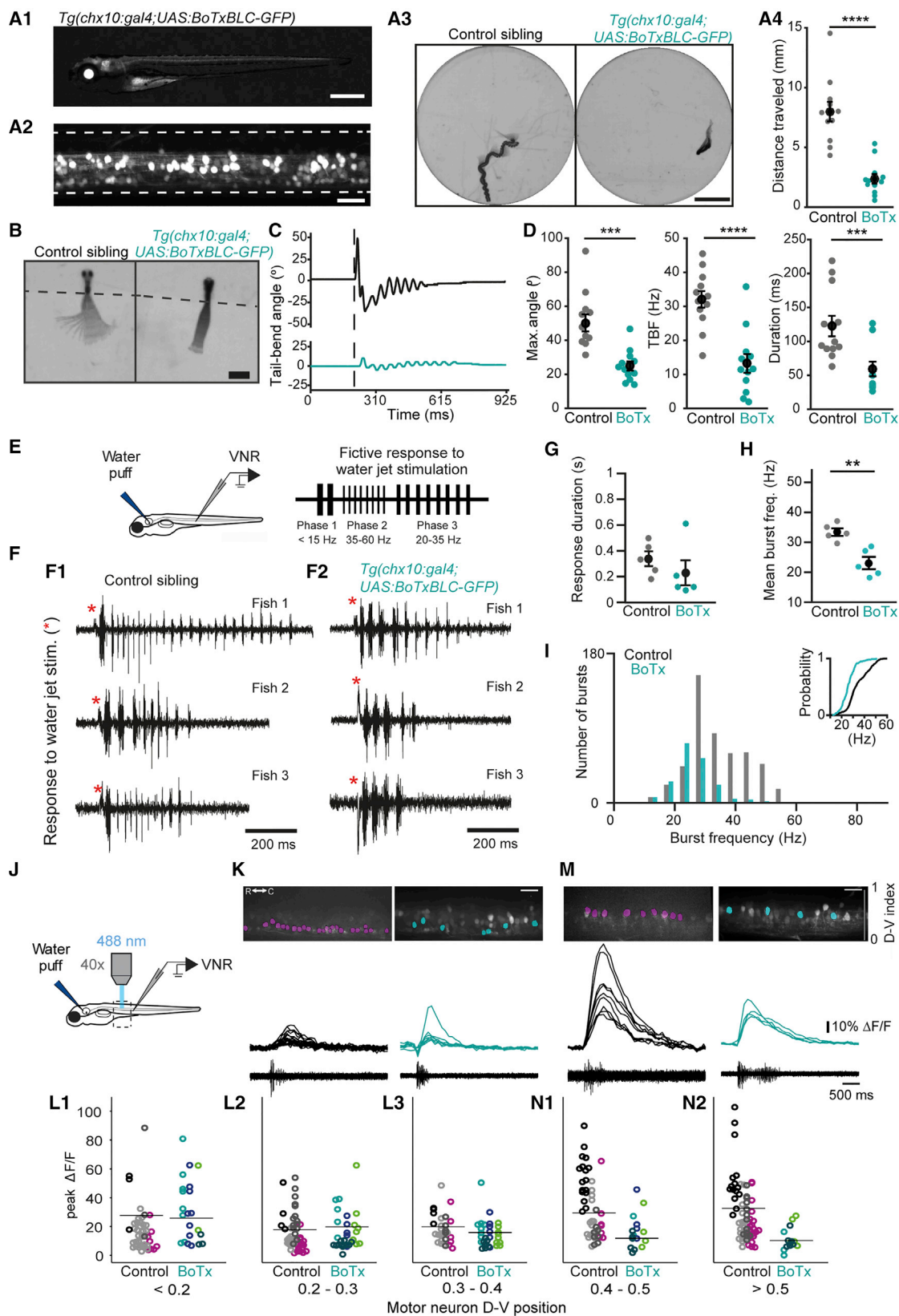
(A) Expression of BoTxBLC-GFP and ChR2-mCherry in *Tg(pkcd211:gal4; UAS:BoTxBLC-GFP; UAS:ChR2-mCherry)*. GFP and mCherry co-labeling in a CSF-cN innervating a CaP primary motor neuron is shown (innervation of a CaP by a CSF-cN is indicated by an arrowhead). (B) Full field light-mediated activation of CSF-cNs in *Tg(pkcd211:gal4; UAS:ChR2-mCherry)* induces a monosynaptic IPSC in a CaP that is reduced by gabazine. (B1) is a schematic representation of light-mediated activation of ChR2⁺ CSF-cNs coupled with a whole-cell recording of a CaP (gray) and the average of ten trials (black) are shown in the top panel of (B2); the bottom panel shows that gabazine strongly reduces the induced IPSC (individual traces from one CaP [gray] and the average of ten trials [purple]). (C) No IPSC was observed after light-mediated activation of CSF-cNs in *Tg(pkcd211:gal4; UAS:ChR2-mCherry; UAS:BoTxBLC-GFP)* larvae. (C1) shows the schematic representation of experimental setup. (C2) shows individual traces from one CaP (gray) and the average of ten trials (teal). (D and E) Confirmation of CaP identity after filling with Alexa 488 dye. (D) shows a cell body with Alexa 488 (top), ChR2-mCherry (middle), merge (bottom), and axonal projections onto ventral musculature in (E) (black double arrowhead, CaP soma; double white arrowhead, axon exiting the spinal cord). (F) Quantification of peak IPSC amplitude in control and BoTxBLC-GFP⁺ larvae (control, n = 3 cells from three larvae, 60 trials; gabazine, n = 2 cells from two larvae, 40 trials; BoTxBLC-GFP⁺, n = 3 cells from three larvae, 60 trials). (A) and (E) are z projection stacks from a few optical sections imaged on the lateral side. (D) is a single plane image. All images are oriented with rostral to the left and dorsal up. Scale bars represent 10 μm (approximated in D). The central line on each boxplot is the median value, and the box limits are the 25th and 75th percentiles. The whiskers include all data points not considered outliers. *p < 0.05, one-way ANOVA with repeated measures. R, rostral; C, caudal; D dorsal; V, ventral. See also [Figure S2](#) and [Table S1](#).

data) that were strongly reduced by bath application of GABA_AR antagonist gabazine (Figure 2B2). In *Tg(pkcd211:gal4; UAS:BoTxBLC-GFP; UAS:ChR2-mCherry)* larvae, light-mediated spiking in CSF-cNs did not generate IPSCs in CaPs (Figure 2C). The identity of the CaP was confirmed by filling the cells with Alexa 488 dye (Figures 2D and 2E). In 59 out of 60 trials, expression of BoTxBLC-GFP abolished the evoked current in CaPs (Figure 2F). Despite the block of synaptic release, *Tg(pkcd211:gal4; UAS:BoTxBLC-GFP)* transgenic larvae did not exhibit any defects in spinal cord formation (Figure S2). Furthermore, CSF-cNs retained their standard morphology, and the animals lived to adulthood (data not shown). These results demonstrate the

complete loss of vesicular release from BoTxBLC-GFP-expressing neurons in vivo.

BoTxBLC-Mediated Silencing of V2a Interneurons Confirms Their Critical Role in Fast Locomotion

V2a interneurons are known to drive motor neuron activation, and their recruitment is frequency dependent during fictive locomotion [8, 9, 14]. Therefore, we tested how V2a silencing impacts fast and slow locomotor regimes during active locomotion. Expression of BoTxBLC-GFP under the control of the *chx10* promoter [5] targeted most V2a interneurons (Figures 3A1 and 3A2). Consequently, acoustic escape responses in these larvae



(legend on next page)

showed a large reduction in the distance traveled in responsive trials compared to control siblings (Figures 3A3 and 3A4; Movie S3). In *Tg(chx10:gal4; UAS:BoTxBLC-GFP)* larvae assayed in a head-embedded and tail-free configuration (Figures 3B–3C; Movie S4), the maximum bend angle, average tail-beat frequency, and response duration were all significantly reduced compared to control siblings during the acoustic escape response (Figure 3D).

Although the *Tg(chx10:gal4)* transgenic line recapitulated *chx10* expression in the hindbrain and rostral spinal cord [5], a few neurons with axons exiting the spinal cord were labeled caudally (Figure 3A2), which could contribute to the response by affecting muscle contraction. To circumvent this confound, we performed fictive ventral nerve root (VNR) recordings in 4 dpf paralyzed larvae, which allowed monitoring of the motor neuron output upstream of the neuromuscular junction. In control siblings, fast escape responses induced by otic vesicle stimulation [32] consisted of a few large amplitude bursts (phase 1), followed by fast-frequency swimming (~35–60 Hz; phase 2), which transitioned to slow-frequency swimming (<35 Hz; phase 3) (Figure 3E). Silencing of V2a output selectively disrupted fast swimming (Figure 3F); the response duration was not significantly reduced (Figure 3G). Fast locomotor frequencies above 40 Hz were abolished, whereas lower frequencies were unaffected (Figures 3H and 3I).

Motor neurons are incrementally recruited along the dorsoventral axis with swimming frequency [7]. To investigate how motor neuron recruitment was affected when V2as were silenced, we generated a novel transgenic line, *Tg(mnx1:GCaMP5G)*, in which

motor neurons express the genetically encoded calcium sensor GCaMP5G, and coupled calcium imaging of motor neurons with otic-vesicle stimulation and VNR recordings [28, 33] (Table S1; Experimental Procedures; Figures 3J–3N). The amplitude of calcium transients varied as a function of the dorsoventral position within the motor pool in a different manner for control *Tg(mnx1:GCaMP5G)* larvae and V2a-silenced *Tg(mnx1:GCaMP5G; chx10:gal4; UAS:BoTxBLC-GFP)* larvae (Figures 3K and 3M; $p = 0.000005$). Overall, the average peak $\Delta F/F$ amplitude was highest in the most dorsal motor neurons in control larvae. Ventral motor neurons exhibited similar $\Delta F/F$ amplitude whether V2as were silenced or not (Figure 3L). In contrast, the activity of dorsal motor neurons was largely reduced in V2a-silenced larvae compared to controls (Figure 3N). A reduction in the recruitment of dorsal motor neuron is consistent with our observations that fast locomotor frequencies (>40 Hz) in both active and fictive locomotion are abolished when V2as are silenced.

Silencing of V2a Interneurons Decreases the Locomotor Frequency during Spontaneous Slow Swimming

Despite the role of hindbrain V2a neurons in initiating locomotion in zebrafish larva [5], the V2a contribution to spontaneous slow swimming has not been directly addressed. In freely swimming larvae, we noted that the occurrence of spontaneous slow swimming was largely reduced in *Tg(chx10:gal4; UAS:BoTxBLC-GFP)* (Figures 4A–4D; Movie S5), indicating that these neurons normally drive spontaneous locomotion. We observed that the rarely occurring swim bouts were on average longer in duration (Figure 4E). In V2a-silenced larvae, fictive

Figure 3. V2a Interneurons Are Critical for Induced Fast-Frequency Swimming

- (A) Comparison of control siblings and *Tg(chx10:gal4; UAS:BoTxBLC-GFP)* 5 dpf larvae in a freely swimming acoustic escape assay. Whole-larva lateral view (A1), lateral view of the spinal cord with borders denoted by dotted line (A2), and trajectories of swimming larvae in the assay (A3) are shown. Control siblings are *Tg(UAS:BoTxBLC-GFP)* larvae. (A4) shows the average distance traveled during a responsive trial (in millimeters) ($n = 11$ control larvae, 81 responses out of 120 trials; $n = 12$ BoTxBLC-GFP⁺ larvae, 107 responses out of 120 trials).
- (B–D) Comparison of control siblings and *Tg(chx10:gal4; UAS:BoTxBLC-GFP)* 5 dpf larvae in a head-embedded, tail-free acoustic escape assay. (B) Left: control larva (*Tg(UAS:BoTxBLC-GFP)*). Right: *Tg(chx10:gal4; UAS:BoTxBLC-GFP)* larva with its head embedded in agarose and the tail free to move. The dotted line indicates the agar border. (C) Example tail-bend angle (degrees) extracted for head-restrained control larvae (*Tg(UAS:BoTxBLC-GFP)* alone, black, top) and BoTxBLC-GFP (*Tg(chx10:gal4; UAS:BoTxBLC-GFP)*), teal, bottom). The dotted line indicates the time of stimulus delivery. (D) Kinematic analysis of head-embedded acoustic-induced escape responses. Maximum bend angle in the trial (left, degrees), average tail-beat frequency within a bout (center, Hz), and average bout duration (right, ms). $n = 12$ control larvae, 104 trials; $n = 12$ *Tg(chx10:gal4; UAS:BoTxBLC-GFP)* larvae, 118 trials.
- (E–I) Analysis of fictive VNR recordings during escape responses in 4 dpf larvae. (E) Left: schematic of the otic vesicle stimulation used to evoke fast escape responses in combination with fictive VNR recordings. Right: three phases of the response can be distinguished in the escape response. (F) Representative traces of fictive escape responses from three larvae for control (F1) and *Tg(chx10:gal4; UAS:BoTxBLC-GFP)* (F2) larvae. Red asterisks indicate the stimulus onset. (G and H) Response duration (G, s) and mean burst frequency (H, Hz) for $n = 57$ stimulations for five control larvae and $n = 54$ stimulations for five BoTxBLC-GFP⁺ larvae. (I) Distribution of burst frequencies (Hz) in control larvae (gray) and BoTxBLC-GFP⁺ larvae (teal). Inset: cumulative distribution function.
- (J–N) Calcium transients, imaged in motor neurons as a function of dorsoventral position, when V2as are silenced (BoTxBLC-GFP⁺) or not (control) with simultaneous fictive VNR recording. (J) Schematic of the calcium imaging configuration performed in combination with otic vesicle stimulation and VNR recordings as described in (E). (K) GCaMP5G expression in *Tg(mnx1:GCaMP5G)* with ROIs overlaid (top), calcium transients (center), and fictive VNR recording during a fictive escape in ventral motor neurons (bottom). Control larva: purple ROIs, black $\Delta F/F$ trace (left). BoTxBLC-GFP⁺ larva: teal ROIs, teal $\Delta F/F$ trace (right). (L) Peak $\Delta F/F$ response for an individual ROI, color-coded by larva, with the average across larvae indicated by a black line. Comparison of control versus BoTxBLC-GFP⁺ larvae for ventral motor neurons at dorsoventral positions: 0–0.2 (L1), 0.2–0.3 (L2), or 0.3–0.4 (L3). (M) Same as (K) but for dorsal motor neurons. (N) Same as (L) but for dorsoventral positions: 0.4–0.5 (N1) or 0.5–1 (N2).

For (L) and (N), $n = 199$ ROIs from 55 stimulations with swimming episodes for five control larvae and $n = 102$ ROIs from $n = 30$ stimulations with swimming episodes for four BoTxBLC-GFP⁺ larvae. Scale bars represent 100 μm in (A1), 25 μm in (A2), 5 mm in (A3), 1 mm in (B), and 20 μm in (K) and (M). For (A4), (D), (G), and (H), each data point is the average across all trials for a single larva. Control sibling *Tg(UAS:BoTxBLC-GFP)* larvae are in gray and *Tg(chx10:gal4; UAS:BoTxBLC-GFP)* are in teal. Means are shown \pm SEM in black. ** $p < 0.01$, *** $p < 0.001$, **** $p < 0.0001$. See also Table S1 and Movies S3 and S4.

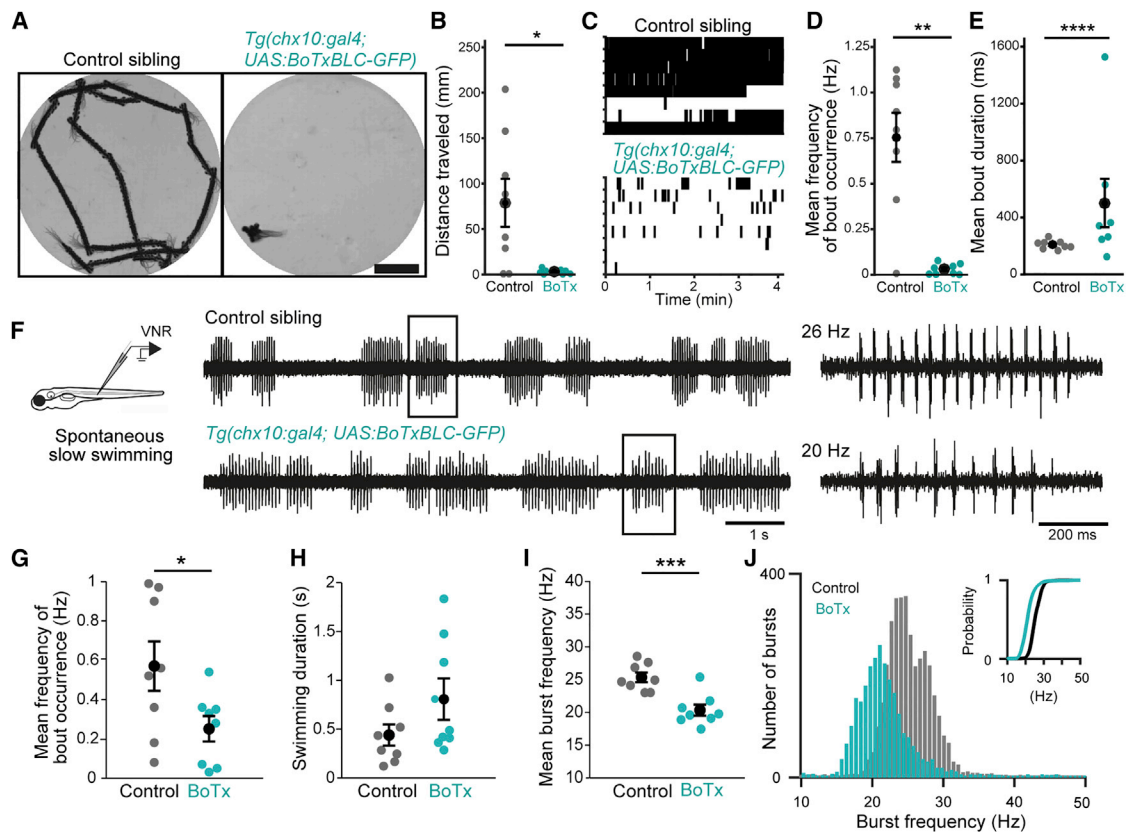


Figure 4. V2a Interneurons Drive Most of Spontaneous Slow Swimming and Adjust the Locomotor Frequency in the Slow Regime

(A–E) Spontaneous slow swimming assay comparing control and *Tg(chx10:gal4; UAS:BoTxBLC-GFP)* larvae at 5 dpf.

(A) The trajectory of a 5 dpf larvae spontaneously swimming for the first minute of a 4 min recording. Left: control sibling (*Tg(UAS:BoTxBLC-GFP)*) alone. Right: *Tg(chx10:gal4; UAS:BoTxBLC-GFP)* larva recorded simultaneously.

(B) Average distance traveled (mm; measured during the first minute of the trial).

(C) Rastergram of the timing of swim bout initiation over the 4 min spontaneous swimming trial recorded. The y axis represents a different individual larva. Top: control siblings. Bottom: *Tg(chx10:gal4; UAS:BoTxBLC-GFP)*.

(D) Mean frequency of bout occurrence (bouts per second, Hz) measured over a 4 min trial.

(E) Average bout duration (ms) across all bouts recorded spontaneously in a 4 min trial.

(B–E) $n = 8$ control larvae and $n = 8$ BoTxBLC-GFP⁺ larvae.

(F) Schematic and example trace of fictive slow swimming in a control (top) and a BoTxBLC-GFP⁺ (bottom) larva. Boxes indicate expanded regions at right. Note the reduced burst frequency in BoTxBLC-GFP⁺ larvae when V2as are silenced.

(G) Reduction in frequency of bout occurrence (bouts per second) in BoTxBLC-GFP⁺ larvae compared to control siblings ($n = 1265$ bouts for eight control larvae; $n = 938$ bouts for eight BoTxBLC-GFP⁺ larvae).

(H) Fictive bout duration (s).

(I) Mean burst frequency during fictive slow swim bouts (Hz).

(H and I) $n = 741$ bouts from eight control larvae; $n = 497$ bouts from eight BoTxBLC-GFP⁺ larvae.

(J) Distribution of burst frequencies (Hz) in control larvae (gray) and BoTxBLC-GFP⁺ larvae (teal). Inset: cumulative distribution function.

For (B), (D), (E), (G), (H), and (I), control siblings (gray, *Tg(UAS:BoTxBLC-GFP)*) were compared to *Tg(chx10:gal4; UAS:BoTxBLC-GFP)* larvae (teal), and each point represents a single larva. Means are shown \pm SEM in black. * $p < 0.05$, ** $p < 0.01$, *** $p < 0.001$, **** $p < 0.0001$, Student's *t* test (D and G). See also [Table S1](#) and [Movie S5](#).

slow swim bouts occurred less frequently and tended to last longer than in control siblings (Figures 4F–4H). In contrast to fast escapes, in which a reduction of frequency occurred via a suppression of the highest frequencies (Figure 3I), in the slow regime swim frequency was reduced by a downward shift of locomotor frequencies (Figures 4I and 4J). Taken together, the active and fictive data demonstrate that V2a interneurons contribute to generation of spontaneous swim events and setting the range of locomotor frequencies during slow locomotion.

DISCUSSION

Silencing with the Optimized Botulinum Toxin Light Chain

Silencing large populations of neurons in vivo is critical to understanding their role in circuits that control behavior. To be readily implemented, silencing tools should be genetically encoded, efficient, and non-toxic. BoTxBLC-GFP is efficient at blocking presynaptic vesicular release, as demonstrated here by probing monosynaptically connected pairs of neurons in vivo.

Neurotoxins have been used extensively for eliminating neuronal activity. Persistent problems for diphtheria use include off-target damage and establishing stable transgenic lines, while in the case of tetanus, detection of fluorescence is difficult *in vivo* [19, 34–36]. The stable transgenic BoTxBLC-GFP has been effective for many generations, and fluorescence could be detected *in vivo*. Codon optimization of BoTxBLC-GFP was critical for expression and silencing in zebrafish, demonstrating the need to design model-specific tools.

Other strategies such as Nitroreductase, KillerRed, or transient receptor potential channels developed for targeted cell ablation or silencing in zebrafish work *in vivo* but require a chemical cofactor or light delivery [34–37]. With chemically mediated methods, ablations can require long incubation times, depending on the expression level, and if driver lines express in non-neuronal tissues [36], these tissues will be ablated. Although opsins can silence with precise spatial and temporal resolution, light delivery can interfere with light-sensitive behaviors, and opsins are currently unfeasible for silencing across large spatial regions during active behavior because they require high power density [38–40]. BoTxBLC-GFP offers a straightforward alternative to these existing methods, potently and chronically silencing in neuronal tissue without additional cofactors or off-target effects. Implementing inducible expression in the future would allow dissection of the relative contributions of acute versus chronic silencing.

The Contribution of V2a Interneurons to Locomotion

chx10⁺ V2a glutamatergic neurons are involved in initiation [5], termination [6], left-right alternation [41], and setting of locomotor frequency [7, 11, 42] in vertebrate species. V2a interneurons recorded during fictive locomotion in zebrafish are recruited in a frequency-dependent manner along the dorsoventral axis and are necessary for generation of high-frequency swimming [8, 12]. Here we investigated the effects of silencing a majority of V2as during two motor behaviors: slow spontaneous swimming and fast escape responses. The escape response in zebrafish larva includes a wide range of locomotor frequencies from 15–100 Hz [2, 43]. Fast components of the escape were suppressed when V2a interneurons were silenced, confirming the critical role of V2as in fast locomotion [8, 44]. By performing calcium imaging on the motor pool, we showed that this suppression effect corresponds to the diminished recruitment of dorsal motor neurons essential for fast swimming. This suggests that the excitation of motor neurons by V2as is necessary to generate fast locomotor frequencies.

Spontaneous slow locomotion occurs in a narrow range of locomotor frequencies (20–30 Hz) [2, 43], during which a subset of ventral V2as is active [8]. Spontaneous active slow swimming rarely occurred when V2as were silenced, and those swim bouts lasted longer. These effects could be related to hindbrain V2a populations involved in initiating locomotion [5] or controlling the duration of locomotor events [6]. In addition, we observed that V2as adjust the locomotor frequency in the slow regime. Further investigation should clarify how excitation by V2as from the hindbrain and spinal cord contribute to this effect. The remaining source of excitation driving slow swimming when V2as are silenced could be glutamatergic V0-v neurons, referred to as MCoDs in zebrafish, which are selectively recruited

at these frequencies [8], suggesting that MCoDs and V2as may work in concert during slow locomotion.

Our results confirm important contributions for V2as in fast and slow regimes of locomotion. Previous work showed that spinal V2as are a heterogeneous population of neurons based on their dorsoventral positioning, morphology, intrinsic properties, and connectivity [8, 9, 12]. Our results, obtained by silencing of the V2a population in the hindbrain and spinal cord, indicate speed-dependent roles for V2as. Although V2as are critical for sustaining fast locomotion, they appear to adjust locomotor frequency and modulate bout duration in the slow regime. New genetic tools will be required to distinguish how hindbrain and spinal cord V2as accomplish these unique functions.

EXPERIMENTAL PROCEDURES

Generation of Stable Transgenic Zebrafish Lines

25 ng μl^{-1} of *Tol2* transposase mRNA and either *pT2S-UAS:zBoTxBLC-GFP* or *pT2S-UAS:zBoTxBLC* were co-injected into one-cell-stage embryos of the TAB (AB/TUB) strain. 188 injected embryos from seven unique clutches were raised. 47 embryos injected with *pT2S-UAS:zBoTxBLC-GFP* were screened after mating with selected Gal4FF lines for behavioral phenotypes and GFP fluorescence. 13 embryos injected with *pT2S-UAS:zBoTxBLC* were screened by PCR. We used Gal4FF drivers (*Tg(SAGFF73A)* and others) for screening the UAS founder fish. We selected six founders, identified single integrations by Southern blot, and mapped the integration sites from F1 progeny (834 F1 fish examined). A single homozygous F2 line, *Tg(UAS:zBoTxBLC-GFP)34b*, has been stably maintained for over ten generations and used for the experiments shown for all figures except Figure 1C. The sequences are available on the zTrap database (<http://kawakami.lab.nig.ac.jp/ztrap/>). The *Tg(mnx1:GCaMP5G)icm25* stable transgenic line was generated based on the *mnx1* promoter [33] integrated in a 5' entry gateway clone [45] and combined to the pME-GCaMP5G and the 3' polyA entry clone into the destination vector carrying *tol2* sites and *cryaa:venus* [46]. Table S1 lists all transgenic lines used in this study, long-form names, and expression patterns if applicable.

All procedures were approved by the Institut du Cerveau et de la Moelle Épinrière (ICM) and the National Ethics Committee (Comité National de Réflexion Ethique sur l'Expérimentation Animale Ce5/2011/056) based on EU legislation or were in accordance with institutional and national guidelines and regulations at the National Institute of Genetics in accordance with the Guide for the Care and Use of Laboratory Animals of the Institutional Animal Care and Use Committee (IACUC, approval identification number 27-2) in Japan.

ACCESSION NUMBERS

The accession number for the transgenic UAS:BoTxBLC-GFP reported in this paper is ZFIN: ZDB-ALT-160119-9. The accession number for the transgenic *mnx1:GCaMP5G* reported in this paper is ZFIN: ZDB-ALT-160427-5.

SUPPLEMENTAL INFORMATION

Supplemental Information includes Supplemental Experimental Procedures, two figures, one table, and five movies and can be found with this article online at <http://dx.doi.org/10.1016/j.cub.2016.06.037>.

AUTHOR CONTRIBUTIONS

M.S. generated the BoTx constructs and lines in K.K.'s lab, which provided the fish facility and technical assistance to map the integration. M.S. conceived and initiated the BoTx project and generated the plasmid constructs and the stable transgenic line *Tg(UAS:BoTxBLC-GFP)*. M.S. actively worked to validate and maintain active carriers over generations from the line used in this manuscript. J.R.S., K.E.S., and C.W. conceived this study with input from

K.F. J.R.S. performed and analyzed coiling experiments, *in vivo* patch recordings, calcium imaging, VNR recordings, and cell counting. K.E.S. performed and analyzed larval behavioral experiments with help from Y.A. K.F. performed and analyzed VNR recordings. J.G. generated the *Tg(mnx1:GCaMP5G)* transgenic line. H.I. provided the original clones for BoTxLC serotypes. J.H. provided unpublished essential electrophysiological data. C.W. and K.K. supervised the research. J.R.S., K.E.S., and C.W. wrote and revised the manuscript with feedback from K.F., K.K., and M.S.

ACKNOWLEDGMENTS

We thank Professor Shin-Ichi Higashijima for the *Tg(chx10:gal4)* line; Professor Shunji Kozaki for bacterial BoTx plasmids; Dr. Tom Auer and Dr. Filippo Del Bene for the *mnx1* promoter; Professor David McLean for useful feedback; Urs Böhm, Dr. Andrew Prendergast, and Dr. Steven Knafo for support with behavior and tracking; Vincent Guillemot for assistance with statistics; Sophie Nunes Figueiredo, Natalia Maties, and Bogdan Buzurin for fish care; Drs. Ruben Portugues, Ana Faustino, and David Lyons for helpful comments on the manuscript; and the Plateforme d'Imagerie Cellulaire Pitié-Salpêtrière, cloning facility, and biostatistics facility at ICM. This work received support from the JSPS postdoc fellowship (M.S.), National BioResource Project and 15H02370 from MEXT of Japan (K.K.), The Philippe Foundation (C.W., K.E.S., and J.M.H.), and the Chaire d'Excellence of the Ecole des Neurosciences de Paris (E.N.P.), European Research Council starting grant Optoloco no. 311673, and NIH Brain Initiative grant no. 5U01NS090501 (C.W.).

Received: February 19, 2016

Revised: May 24, 2016

Accepted: June 17, 2016

Published: August 11, 2016

REFERENCES

- Severi, K.E., Portugues, R., Marques, J.C., O'Malley, D.M., Orger, M.B., and Engert, F. (2014). Neural control and modulation of swimming speed in the larval zebrafish. *Neuron* 83, 692–707.
- Budick, S.A., and O'Malley, D.M. (2000). Locomotor repertoire of the larval zebrafish: swimming, turning and prey capture. *J. Exp. Biol.* 203, 2565–2579.
- Talpalar, A.E., Bouvier, J., Borgius, L., Fortin, G., Pierani, A., and Kiehn, O. (2013). Dual-mode operation of neuronal networks involved in left-right alternation. *Nature* 500, 85–88.
- Gosgnach, S., Lanuza, G.M., Butt, S.J., Saueressig, H., Zhang, Y., Velasquez, T., Riethmacher, D., Callaway, E.M., Kiehn, O., and Goulding, M. (2006). V1 spinal neurons regulate the speed of vertebrate locomotor outputs. *Nature* 440, 215–219.
- Kimura, Y., Satou, C., Fujioka, S., Shoji, W., Umeda, K., Ishizuka, T., Yawo, H., and Higashijima, S. (2013). Hindbrain V2a neurons in the excitation of spinal locomotor circuits during zebrafish swimming. *Curr. Biol.* 23, 843–849.
- Bouvier, J., Caggiano, V., Leiras, R., Caldeira, V., Bellardita, C., Balueva, K., Fuchs, A., and Kiehn, O. (2015). Descending command neurons in the brainstem that halt locomotion. *Cell* 163, 1191–1203.
- McLean, D.L., Fan, J., Higashijima, S., Hale, M.E., and Fetcho, J.R. (2007). A topographic map of recruitment in spinal cord. *Nature* 446, 71–75.
- McLean, D.L., Masino, M.A., Koh, I.Y., Lindquist, W.B., and Fetcho, J.R. (2008). Continuous shifts in the active set of spinal interneurons during changes in locomotor speed. *Nat. Neurosci.* 11, 1419–1429.
- Menelaou, E., VanDunk, C., and McLean, D.L. (2014). Differences in the morphology of spinal V2a neurons reflect their recruitment order during swimming in larval zebrafish. *J. Comp. Neurol.* 522, 1232–1248.
- Dougherty, K.J., and Kiehn, O. (2010). Functional organization of V2a-related locomotor circuits in the rodent spinal cord. *Ann. N Y Acad. Sci.* 1198, 85–93.
- Ljunggren, E.E., Haupt, S., Ausborn, J., Ampatzis, K., and El Manira, A. (2014). Optogenetic activation of excitatory premotor interneurons is sufficient to generate coordinated locomotor activity in larval zebrafish. *J. Neurosci.* 34, 134–139.
- Ampatzis, K., Song, J., Ausborn, J., and El Manira, A. (2014). Separate microcircuit modules of distinct v2a interneurons and motoneurons control the speed of locomotion. *Neuron* 83, 934–943.
- Ritter, D.A., Bhatt, D.H., and Fetcho, J.R. (2001). *In vivo* imaging of zebrafish reveals differences in the spinal networks for escape and swimming movements. *J. Neurosci.* 21, 8956–8965.
- Kimura, Y., Okamura, Y., and Higashijima, S. (2006). *alx*, a zebrafish homolog of *Chx10*, marks ipsilateral descending excitatory interneurons that participate in the regulation of spinal locomotor circuits. *J. Neurosci.* 26, 5684–5697.
- Kao, I., Drachman, D.B., and Price, D.L. (1976). Botulinum toxin: mechanism of presynaptic blockade. *Science* 193, 1256–1258.
- Schiavo, G., Benfenati, F., Poulain, B., Rossetto, O., Poverino de Laureto, P., DasGupta, B.R., and Montecucco, C. (1992). Tetanus and botulinum-B neurotoxins block neurotransmitter release by proteolytic cleavage of synaptobrevin. *Nature* 359, 832–835.
- Sutton, R.B., Fasshauer, D., Jahn, R., and Brunger, A.T. (1998). Crystal structure of a SNARE complex involved in synaptic exocytosis at 2.4 Å resolution. *Nature* 395, 347–353.
- Brunger, A.T., Jin, R., and Breidenbach, M.A. (2008). Highly specific interactions between botulinum neurotoxins and synaptic vesicle proteins. *Cell. Mol. Life Sci.* 65, 2296–2306.
- Asakawa, K., Suster, M.L., Mizusawa, K., Nagayoshi, S., Kotani, T., Urasaki, A., Kishimoto, Y., Hibi, M., and Kawakami, K. (2008). Genetic dissection of neural circuits by Tol2 transposon-mediated Gal4 gene and enhancer trapping in zebrafish. *Proc. Natl. Acad. Sci. USA* 105, 1255–1260.
- Scott, E.K., Mason, L., Arrenberg, A.B., Ziv, L., Gosse, N.J., Xiao, T., Chi, N.C., Asakawa, K., Kawakami, K., and Baier, H. (2007). Targeting neural circuitry in zebrafish using GAL4 enhancer trapping. *Nat. Methods* 4, 323–326.
- Fidelin, K., Djenoune, L., Stokes, C., Prendergast, A., Gomez, J., Baradel, A., Del Bene, F., and Wyart, C. (2015). State-dependent modulation of locomotion by GABAergic spinal sensory neurons. *Curr. Biol.* 25, 3035–3047.
- Saint-Amant, L., and Drapeau, P. (1998). Time course of the development of motor behaviors in the zebrafish embryo. *J. Neurobiol.* 37, 622–632.
- Saint-Amant, L., and Drapeau, P. (2000). Motoneuron activity patterns related to the earliest behavior of the zebrafish embryo. *J. Neurosci.* 20, 3964–3972.
- Warp, E., Agarwal, G., Wyart, C., Friedmann, D., Oldfield, C.S., Conner, A., Del Bene, F., Arrenberg, A.B., Baier, H., and Isacoff, E.Y. (2012). Emergence of patterned activity in the developing zebrafish spinal cord. *Curr. Biol.* 22, 93–102.
- Wyart, C., Del Bene, F., Warp, E., Scott, E.K., Trauner, D., Baier, H., and Isacoff, E.Y. (2009). Optogenetic dissection of a behavioural module in the vertebrate spinal cord. *Nature* 461, 407–410.
- Djenoune, L., Khabou, H., Joubert, F., Quan, F.B., Nunes Figueiredo, S., Bodineau, L., Del Bene, F., Burcklé, C., Tostivint, H., and Wyart, C. (2014). Investigation of spinal cerebrospinal fluid-contacting neurons expressing PKD2L1: evidence for a conserved system from fish to primates. *Front. Neuroanat.* 8, 26.
- Lauterbach, M.A., Ronzitti, E., Sternberg, J.R., Wyart, C., and Emiliani, V. (2015). Fast calcium imaging with optical sectioning via HiLo microscopy. *PLoS ONE* 10, e0143681.
- Akerboom, J., Chen, T.W., Wardill, T.J., Tian, L., Marvin, J.S., Mutlu, S., Calderón, N.C., Esposti, F., Borghuis, B.G., Sun, X.R., et al. (2012). Optimization of a GCaMP calcium indicator for neural activity imaging. *J. Neurosci.* 32, 13819–13840.
- Kohashi, T., Nakata, N., and Oda, Y. (2012). Effective sensory modality activating an escape triggering neuron switches during early development in zebrafish. *J. Neurosci.* 32, 5810–5820.

30. Böhm, U.L., Prendergast, A., Djenoune, L., Nunes Figueiredo, S., Gomez, J., Stokes, C., Kaiser, S., Suster, M., Kawakami, K., Charpentier, M., et al. (2016). CSF-contacting neurons regulate locomotion by relaying mechanical stimuli to spinal circuits. *Nat. Commun.* 7, 10866.
31. Satou, C., Kimura, Y., Hirata, H., Suster, M.L., Kawakami, K., and Higashijima, S. (2013). Transgenic tools to characterize neuronal properties of discrete populations of zebrafish neurons. *Development* 140, 3927–3931.
32. Kohashi, T., and Oda, Y. (2008). Initiation of Mauthner- or non-Mauthner-mediated fast escape evoked by different modes of sensory input. *J. Neurosci.* 28, 10641–10653.
33. Zelenchuk, T.A., and Brusés, J.L. (2011). In vivo labeling of zebrafish motor neurons using an *mx1* enhancer and Gal4/UAS. *Genesis* 49, 546–554.
34. Lee, A., Mathuru, A.S., Teh, C., Kibat, C., Korzh, V., Penney, T.B., and Jesuthasan, S. (2010). The habenula prevents helpless behavior in larval zebrafish. *Curr. Biol.* 20, 2211–2216.
35. Curado, S., Anderson, R.M., Jungblut, B., Mumm, J., Schroeter, E., and Stainier, D.Y. (2007). Conditional targeted cell ablation in zebrafish: a new tool for regeneration studies. *Dev. Dyn.* 236, 1025–1035.
36. Curado, S., Stainier, D.Y., and Anderson, R.M. (2008). Nitroreductase-mediated cell/tissue ablation in zebrafish: a spatially and temporally controlled ablation method with applications in developmental and regeneration studies. *Nat. Protoc.* 3, 948–954.
37. Chen, S., Chiu, C.N., McArthur, K.L., Fetcho, J.R., and Prober, D.A. (2016). TRP channel mediated neuronal activation and ablation in freely behaving zebrafish. *Nat. Methods* 13, 147–150.
38. Mattis, J., Tye, K.M., Ferenczi, E.A., Ramakrishnan, C., O’Shea, D.J., Prakash, R., Gunaydin, L.A., Hyun, M., Fenno, L.E., Gradinaru, V., et al. (2011). Principles for applying optogenetic tools derived from direct comparative analysis of microbial opsins. *Nat. Methods* 9, 159–172.
39. Friedmann, D., Hoagland, A., Berlin, S., and Isacoff, E.Y. (2015). A spinal opsin controls early neural activity and drives a behavioral light response. *Curr. Biol.* 25, 69–74.
40. Rihel, J., and Schier, A.F. (2012). Behavioral screening for neuroactive drugs in zebrafish. *Dev. Neurobiol.* 72, 373–385.
41. Crone, S.A., Quinlan, K.A., Zagoraïou, L., Droho, S., Restrepo, C.E., Lundfald, L., Endo, T., Setlak, J., Jessell, T.M., Kiehn, O., and Sharma, K. (2008). Genetic ablation of V2a ipsilateral interneurons disrupts left-right locomotor coordination in mammalian spinal cord. *Neuron* 60, 70–83.
42. Dougherty, K.J., Zagoraïou, L., Satoh, D., Rozani, I., Doobar, S., Arber, S., Jessell, T.M., and Kiehn, O. (2013). Locomotor rhythm generation linked to the output of spinal *shox2* excitatory interneurons. *Neuron* 80, 920–933.
43. Mirat, O., Sternberg, J.R., Severi, K.E., and Wyart, C. (2013). ZebraZoom: an automated program for high-throughput behavioral analysis and categorization. *Front. Neural Circuits* 7, 107.
44. Eklöf-Ljunggren, E., Haupt, S., Ausborn, J., Dehnisch, I., Uhlén, P., Higashijima, S., and El Manira, A. (2012). Origin of excitation underlying locomotion in the spinal circuit of zebrafish. *Proc. Natl. Acad. Sci. USA* 109, 5511–5516.
45. Kwan, K.M., Fujimoto, E., Grabher, C., Mangum, B.D., Hardy, M.E., Campbell, D.S., Parant, J.M., Yost, H.J., Kanki, J.P., and Chien, C.B. (2007). The Tol2kit: a multisite gateway-based construction kit for Tol2 transposon transgenesis constructs. *Dev. Dyn.* 236, 3088–3099.
46. Ni, T.T., Lu, J., Zhu, M., Maddison, L.A., Boyd, K.L., Huskey, L., Ju, B., Hesselson, D., Zhong, T.P., Page-McCaw, P.S., et al. (2012). Conditional control of gene function by an invertible gene trap in zebrafish. *Proc. Natl. Acad. Sci. USA* 109, 15389–15394.